




Biogeochemical cycling of Cd, Mn, and Ce in the Eastern Tropical North Pacific oxygen-deficient zone

Xiaopeng Bian ^{1,*} Shun-Chung Yang,¹ Kenneth M. Bolster,¹ Rintaro Moriyasu ² James W. Moffett ² Seth G. John¹

¹Department of Earth Sciences, University of Southern California, Los Angeles, California

²Department of Biological Sciences, University of Southern California, Los Angeles, California

Abstract

Oxygen-deficient zones (ODZs) play an important role in the distribution and cycling of trace metals in the ocean, as important sources of metals including Fe and Mn, and also as possible sinks of chalcophile elements such as Cd. The Eastern Tropical North Pacific (ETNP) ODZ is one of the three largest ODZs worldwide. Here, we present results from two sectional surveys through the ETNP ODZ conducted in 2018, providing high-resolution concentrations of several metals, along with complimentary measurements of nutrients and iodine speciation. We show that samples obtained from the ship's regular rosette are clean for Cd, Mn, Ni, and light rare earth elements, while uncontaminated Fe, Zn, Cu, and Pb samples cannot be obtained without a special trace-metal clean sampling system. Our results did not show evidence of Cd sulfide precipitation, even within the most oxygen-depleted water mass. High Mn and Ce concentrations and high Ce anomalies were observed in low-oxygen seawater. These maxima were most pronounced in the upper water column below the oxycline, coincident with the secondary nitrite maxima and the lowest oxygen concentrations, in what is generally considered the most microbially active part of the water column. High Mn and Ce features were also coincident with maxima in excess iodine, a tracer of shelf sediment sources. Mn and Ce maxima were most prominent within the 13°C water mass, spanning a density horizon that enhances isopycnal transport from the shelf sediments, resulting in transport of Mn and Ce at least 2500 km offshore.

Oxygen-deficient zones (ODZs) are regions with extremely low oxygen concentrations in subsurface waters, due to the high primary productivity in surface seawater and the intense subsurface remineralization that consumes oxygen. ODZs play an important role in the global nitrogen cycle as “hot spots” of fixed nitrogen loss and nitrous oxide (N₂O, a potent greenhouse gas) production (Pierotti and Rasmussen 1980; Knowles 1982; Chang et al. 2012). In addition to their crucial

role in the marine nitrogen cycle, ODZs can influence the exchange of metals between continental margins and ocean basins (Lam et al. 2020; Moffett and German 2020). Therefore, it is important to study trace metal cycling in ODZs because many trace metals—including Fe, Mn, Cu, Co, Zn, and Cd—are required as cofactors for various enzymes and are essential micronutrients to phytoplankton, and thus also influence the global carbon and nitrogen cycles (Morel et al. 2003).

ODZs can influence metal cycling in different ways. ODZs are often associated with elevated concentrations of redox-sensitive elements, such as Mn, Fe, Ce, and Co, because their reduced forms are much more soluble than their corresponding oxidized forms in seawater (Moffett and Ho 1996; Liu and Millero 2002; Morton et al. 2019). These redox-sensitive trace metals are often co-enriched in low-oxygen seawater and exhibit similar biogeochemical features. In particular, cerium (Ce) is known to resemble Mn in its marine chemistry (Moffett 1990, 1994). Ce is one of the rare earth elements (REEs). Although most REEs exist in the +3 oxidation state (de Baar et al. 1988), Ce (III) can be microbially oxidized to Ce (IV), followed by preferential scavenging of Ce (IV) from oxic waters by Mn oxidizing bacteria, leading to Ce depletion with respect to its lanthanide neighbors such as La,

*Correspondence: xiaopenb@usc.edu

This is an open access article under the terms of the [Creative Commons Attribution](#) License, which permits use, distribution and reproduction in any medium, provided the original work is properly cited.

Author Contribution Statement: X.B., J.W.M., and S.G.J. designed the study. X.B., S-C.Y., K.M.B., R.M., and J.W.M. equally contributed to the sample collection on the RR1804 and RR1805 cruises. R.M. analyzed iodine speciation of RR1804 samples with the help of K.M.B. and X.B. onboard. X.B. analyzed trace metal samples of RR1804 and S-C.Y. analyzed trace metal samples of RR1805. S.G.J. supervised X.B. S-C.Y., K.M.B., and R.M. contributed to the preparation of this manuscript. X.B. wrote this manuscript and coordinated its distribution between authors. J.W.M. and S.G.J. made significant contributions to the revision of this manuscript. All authors offered feedback and revisions to this manuscript.

Pr, and Nd (Moffett 1990). In ODZs, these redox sensitive elements can be released from shelf sediments and transported by low-oxygen water masses away from the coastlines into the oceans, where they can be an important trace metal source for phytoplankton and alleviate the limitation stress of essential elements, particularly Fe (Bruland et al. 2005; Lam and Bishop 2008; Hawco et al. 2016).

Some trace metals are not redox sensitive, but have been proposed to be influenced by the sulfur cycle in ODZs (Canfield et al. 2010), specifically chalcophile elements that tend to form metal sulfides. This hypothesis—that Cd is lost from water column as Cd sulfide (CdS) in anoxic microenvironments in organic particles—has been most commonly advanced to explain Cd and Cd isotope patterns in ODZs (Janssen et al. 2014; Conway and John 2015a), with implications for understanding both the modern ocean Cd cycle (Roshan and DeVries 2021), and the use of Cd/Ca ratios in foraminiferal records as a paleoceanographic proxy for dissolved phosphate to reconstruct water mass distribution and nutrient utilization in past oceans (Boyle 1988; Elderfield and Rickaby 2000). However, several recent studies reported that CdS precipitation was not observed in other ODZ regions (John et al. 2018; Yang et al. 2018; de Souza et al. 2022), indicating that CdS precipitation is not a driving mechanism that controls the global Cd cycling.

Motivated by the debate about the Cd sulfide hypothesis (Janssen et al. 2014; Conway and John 2015a; de Souza et al. 2022) and previous studies about redox-sensitive metals in ODZs (de Baar et al. 1988; Saager et al. 1989; Vedamati et al. 2015), in this study, we participated on two cruises in the Eastern Tropical North Pacific (ETNP) ODZ to test the CdS hypothesis and examine the distribution and cycling of Mn and Ce. Another main purpose of these cruises was to study the distribution of oxygen and nitrogen chemistry in the region as part of a 50-yr time series study of the biogeochemistry and physical boundaries of the denitrifying regime in the region (Brandes et al. 1998; Fuchsman et al. 2018). Compared with abundant studies on oxygen and nitrogen chemistry, the trace metal data are scarce in the ETNP ODZ. A recent Cd study has also called for higher-resolution data in the ETNP (de Souza et al. 2022). In this study, we adopted a sampling strategy that provided an unprecedented opportunity for high-resolution sampling in the region for trace metal studies. Complimentary measurements of iodine speciation and nitrite are also available (Evans et al. 2020; Moriyasu et al. 2020), providing valuable context for the trace metals studied here. The new high-resolution data presented in this study will provide valuable information to assess the CdS hypothesis and deepen our understanding of the cycling of Cd, Mn, and Ce in the ocean.

Methods

Sampling

The samples were collected during two cruises of the R/V Roger Revelle, RR1804 and RR1805 in the ETNP Ocean,

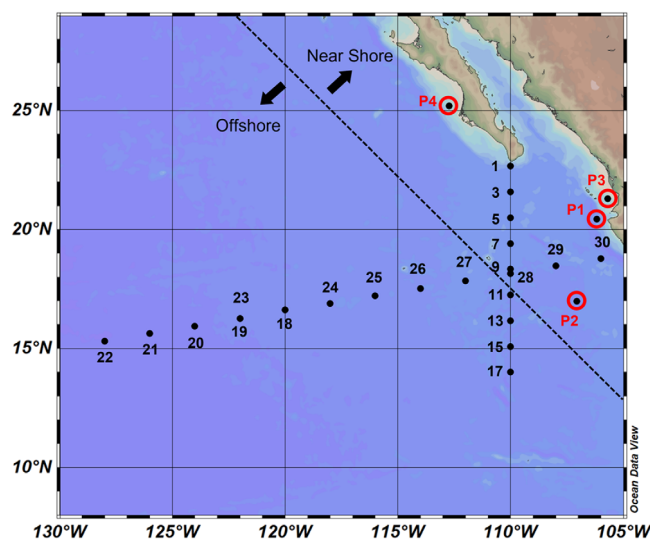


Fig. 1. Seawater sampling locations in the ETNP ODZ. Black dots with numbers are stations from cruise RR1804 where seawater samples were collected using a non-TMC system. The four stations highlighted by red circles, P1, P2, P3, and P4, are stations from cruise RR1805 where seawater samples were collected using TMC techniques. RR1804 stations are split into near-shore and offshore stations based on their distances from the coastline.

23N-14N, 105W-130W, from March to April 2018. The RR1804 cruise was comprised of one zonal and one meridional section (Fig. 1).

The collection of contamination-free seawater can be challenging because of the extremely low concentrations of these elements in seawater, and the ubiquity of these elements in sampling platforms on a ship (e.g., dust, steel hydrowire, brass fittings, etc.) (Bruland and Lohan 2003; Measures et al. 2008). Trace-metal clean (TMC) sampling techniques have been standardized to avoid the contamination during sample collection (De Baar et al. 2008; Measures et al. 2008; Cutter et al. 2017). Such techniques rely on special sampling systems designed specifically for TMC sample collection, including Teflon-coated or metal-free bottles of the GO-FLO (General Oceanics) or external-spring configuration, mounted on a rosette made from titanium or powder-coated aluminum, and deployed from a nonmetallic liquid crystal polymer (e.g., Vectran) or polyethylene line (Measures et al. 2008; Cutter and Bruland 2012; Cutter et al. 2017).

In this study, on RR1804, samples were collected using a regular metal frame CTD rosette equipped with Teflon-coated internal-spring Niskin bottles (12 liters) and analyzed for a suite of metals in the most sampling-intensive phase of the project. Although standard practice for nitrogen cycle work, this sampling system is not designed for the sampling of contamination-prone metals. Each seawater sample was subsampled into a 1-liter acid-cleaned low-density polyethylene (LDPE) bottle on board, and then filtered in a TMC “bubble” in the ship’s TMC van using an AcroPak™ 0.2- μ m filter

and a peristaltic pump, and stored in 50-mL LDPE centrifuge tubes.

On RR1805, TMC sampling technique was used. TMC samples were collected using 5-liter acid-cleaned Teflon-coated external-spring “Niskin-type” bottles (Ocean Test Equipment) on a powder-coated TMC rosette (Sea-Bird Electronics). These Niskins were pressurized with nitrogen and passed through acid-washed 47-mm-diameter 0.2- μm Supor polyethersulfone filters (Pall) into acid-washed 1-liter LDPE bottles (Nalgene). Samples from four stations of the RR1805 cruise (P1, P2, P3, and P4; Fig. 1) were used for inter-comparison with the samples collected from the RR1804 cruise in order to study the “cleanliness” of the non-TMC sampling techniques.

Seawater temperature, salinity, and oxygen concentrations were measured by sensors attached to the non-TMC CTD rosette. The hydrographic and nutrient data of RR1804-RR1805 used in this study are available on BCO-DMO (<http://lod.bco-dmo.org/id/dataset/779185>).

Iodine speciation analysis

Iodide (I^-) and iodate (IO_3^-) were measured for RR1804 samples. After sample collection and filtration, most seawater samples were measured typically within 6 h on board. When samples exceeded the analytical capacity on board, samples were frozen and brought back to the laboratory and measured at USC.

Iodide was analyzed using cathodic square wave stripping voltammetry. Iodate was analyzed using a spectrophotometer (Perkin Elmer Lambda 35) by converting iodate into triiodide (I_3^-) quantitatively in the presence of sulfuric acid and excess iodide. For a detailed description of iodine species analysis, see Moriyasu et al. (2020) and references therein.

The iodide and iodate data were published in Moriyasu et al. (2020) and were used to study trace metal cycling in this study. The iodine speciation data are available on BCO-DMO (<https://www.bco-dmo.org/dataset/776552/data>).

Trace metal analysis

The elements Fe, Zn, Cd, Ni, Cu, Pb, and Mn were measured for both RR1804 and RR1805 samples. Light REEs (LREEs, La to Nd) were only measured for RR1804 samples.

All seawater samples were first acidified to pH 2 with distilled 12 M HCl (the volume ratio of HCl to sample is 1 : 1000) in the clean lab at the University of Southern California (USC). After acidification, seawater samples were stored for at least 3 months before analysis to ensure the complete desorption and dissolution of any metal from the wall of the LDPE tubes or bottles.

Metal concentration analyses were performed as in Hawco et al. (2020) and are briefly summarized below. For each sample, 15 mL seawater was transferred to a 15-mL tube, followed by the addition of 50 μL of an isotope spike (containing ^{57}Fe , ^{62}Ni , ^{65}Cu , ^{67}Zn , ^{207}Pb , and ^{110}Cd) to each

sample tube and thoroughly mixed. The samples were then left to sit overnight before they were preconcentrated by seaFAST™ system. The seaFAST™ system preconcentrates the seawater samples and removes the salt matrix (Lagerström et al. 2013). About 10 mL of seawater was injected through the Nobias PA-1 column on the seaFAST™, and 0.5 mL eluent (1 M HNO_3 containing 1 ppb In) was used to elute trace metals for concentration analysis. The trace metal concentrations were then measured by an Element 2 single collector sector field inductively coupled plasma mass spectrometry (ICP-MS). Concentrations of Fe, Zn, Cd, Ni, Cu, and Pb were calculated using an isotope dilution method. Concentrations of Mn and LREEs were quantified relative to the 10 ppb standard and corrected for incomplete sample loading using the recovery of Ni (Hawco et al. 2020). GEOTRACES standards GSC and GSP were analyzed to assess the accuracy. For all the trace metals analyzed, GSC and GSP values agree well with the values previously reported (Table 1; Hatje et al. 2014; Wuttig et al. 2019; Floback and Moffett 2021). A USC lab working standard (surface seawater from the North Pacific after metal extraction by Nobias-PA1 resin at pH 2) was analyzed repeatedly to monitor the repeatability. For each element, the average and 3 SD values ($n = 47$) are reported (Table 1). The detection limit of each element can be estimated using the 3 SD value. Trace metal concentration results from the RR1804-1805 cruises are available on BCO-DMO (<http://lod.bco-dmo.org/id/dataset/872434>).

Calculation of Cd* and Ce anomaly

In order to study the CdS hypothesis (i.e., Cd is removed from water column as CdS in anoxic microenvironments in organic particles) in the ETNP ODZ, we calculated Cd* to study the relative depletion of Cd compared to phosphate, using the same equation as Janssen et al. (2014):

$$\text{Cd}^* = \text{Cd}_{\text{measured}} - \left(\frac{\text{Cd}}{\text{P}} \right)_{\text{deep}} \times P_{\text{measured}},$$

where $(\text{Cd}/\text{P})_{\text{deep}}$ is the ratio of Cd (expressed in nmol L^{-1}) to phosphate (in $\mu\text{mol L}^{-1}$) in the deep seawater. In this study, $(\text{Cd}/\text{P})_{\text{deep}}$ is set to be $0.317 \text{ nmol } \mu\text{mol}^{-1}$, which is the average Cd/P ratios below 2000 m at the SAFE station in the North Pacific (Conway and John 2015b).

In order to study the degree of Ce depletion relative to other REEs, we calculated the Ce anomaly (Ce/Ce^*) as:

$$\text{Ce}/\text{Ce}^* = \frac{3 \times \text{Ce}_N}{(2 \times \text{La}_N + \text{Nd}_N)},$$

where Ce_N , La_N , and Nd_N are normalized to Post Archean Australian Shale values (McLennan 1989). A lower Ce anomaly value reflects more depletion of Ce relative to the neighboring REEs.

Table 1. Concentrations of trace metals in GEOTRACES standards and the USC lab working standard.

	Fe nmol L ⁻¹	Zn nmol L ⁻¹	Cd nmol L ⁻¹	Ni nmol L ⁻¹	Cu nmol L ⁻¹	Pb pmol L ⁻¹	Mn nmol L ⁻¹	La pmol L ⁻¹	Ce pmol L ⁻¹	Pr pmol L ⁻¹	Nd pmol L ⁻¹
GSP analyzed	—*	0.19	0.014	3.46†	0.71	62.71	0.78	3.85	2.32	0.56	3.53
GSP reference value	0.28‡	0.10‡	0.005‡	2.50‡	0.59‡	64.58‡	0.80‡	3.86‡	2.39‡	0.47‡	3.56‡
GSC analyzed	—*	1.45	0.359	4.34	1.34	38.72	2.05	14.28	12.83	2.47	10.72
GSC reference value	1.55‡	1.45‡	0.359‡	4.01‡	1.17‡	41.00‡	1.99‡	15.04‡	12.49‡	2.99‡	11.03‡
USC lab working standard (mean ± 3 SD)	0.20 ± 0.19	0.43 ± 0.15	0.136 ± 0.016	1.62 ± 0.15	0.16 ± 0.05	62.03 ± 3.69	0.59 ± 0.06	7.86 ± 2.56	2.55 ± 1.07	1.42 ± 0.87	6.91 ± 3.41

*Iron data are missing due to iron contamination during sample analysis.

†Higher Ni concentrations than the consensus value, perhaps due to contamination during analysis.

‡Reference values are from Wuttig et al. (2019), a seawater density of 1.025 kg L⁻¹ was used to convert the unit from nmol (pmol) kg⁻¹ to nmol (pmol) L⁻¹.

§Reference values are from Floback and Moffett (2021).

Results and discussion

Hydrologic background in the ETNP ODZ

The region is characterized by high primary production in surface waters and a strong gradient in oxygen concentrations below the euphotic zone. A broad ODZ is observed in the water column between ~200 and 800 m depth, with [O₂] mostly in the suboxic range (< 5 μmol kg⁻¹) (Fig. 2b). Above the ODZ lies the upper oxycline, between ~50 and 200 m depth (Fig. 2b). The lowest oxygen, and most intense denitrification, occurs in the upper part of this zone (Tiano et al. 2014; Fuchsman et al. 2018). There is a pronounced secondary nitrite maximum in this region over a density range of 26.2 to 26.6. This corresponds with a local maximum in salinity (~34.8 psu) corresponding to the 13°C water mass (13CW) (Fiedler and Talley 2006), a narrow feature which comprises the most microbially active region of denitrification in both the north and south eastern tropical Pacific (Peters et al. 2018; Evans et al. 2020). The situation is complicated because of another water mass, the Northern Equatorial Pacific Intermediate Water (NEPIW), which has a slightly higher oxygen concentration than the 13CW and lies underneath it. The boundary between them can be perturbed by eddies, leading to apparent complexity in nitrite distributions (Evans et al. 2020). The 13CW has outsized importance because the density range from 26.2 to 26.6 intersects with the majority of the continental shelf in Peru and Mexico. The persistence of the water mass facilitates isopycnal transport from waters overlying shelf sediments to the interior of the ODZ. This is apparent for iodide, with a large plume of “excess” iodide (i.e., concentrations exceeding the conservative seawater iodine concentration) forming large offshore plumes (Moriyasu et al. 2020). These excess iodide concentrations were measured on cruise RR1804, providing a direct comparison with the metal concentrations shown here.

Sampling for trace metals with a non-clean system

We collected trace metal samples from the RR1804 cruise using the ship’s regular CTD rosette and Niskin bottles, which is not a standard TMC sampling technique. But previous studies have shown that ship’s regular sampling system can be clean for some trace metals, such as Mn, Cd, and Nd (Janssen et al. 2014; Huang et al. 2021; Zhang et al. 2021). In order to assess the cleanliness of the ship’s regular sampling system, we compared the RR1804 concentrations with those of RR1805—when a TMC sampling technique was used. There are no crossover stations between RR1804 and RR1805. RR1805 stations are all near the shore. So, we split RR1804 samples into near-shore and offshore stations (Fig. 1) and focused more on the comparison between the RR1804 near-shore stations and RR1805 stations. We used two criteria to evaluate the cleanliness of the ship’s regular sampling system: (1) the similarity between concentration profiles from RR1804 and RR1805, and (2) the lowest and highest concentrations

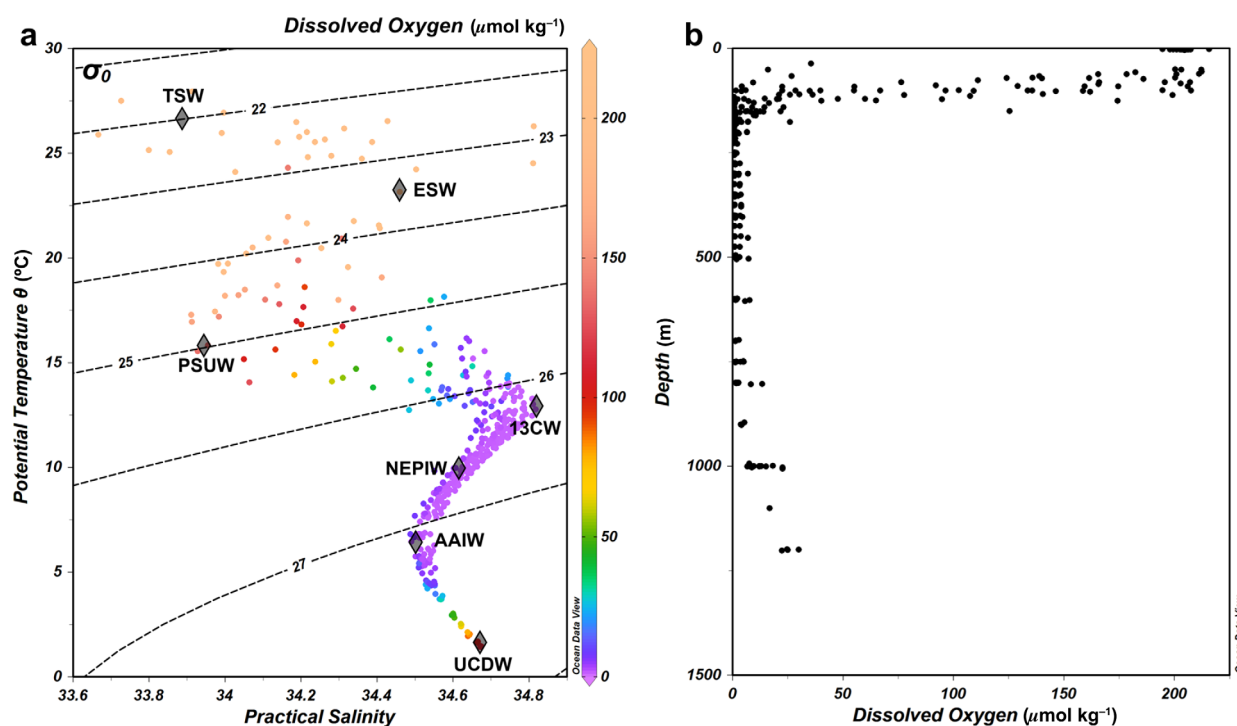


Fig. 2. (a) The T–S diagram of the water samples in this study. Gray diamonds illustrate different water mass end-members in the study region, including Upper Circumpolar Deep Water (UCDW), Antarctic Intermediate Water (AAIW), Northern Equatorial Pacific Intermediate Water (NEPIW), 13°C Water (13CW), Pacific Subarctic Upper Water (PSUW), Equatorial Surface Water (ESW), and Tropical Surface Water (TSW). Colors show the dissolved oxygen concentrations in seawater. (b) The profiles of dissolved oxygen concentrations from all stations of cruise RR1804 in the ETNP ODZ.

measured with each system (Table 2). Based on these two criteria, we found that Cd, Ni, Mn, and LREEs (e.g., Ce) were clean, whereas Fe, Zn, Cu, and Pb were contaminated.

Our results show that the Cd and Ni exhibit typical nutrient-type profiles (Sclater et al. 1976; Bruland 1980; Biller and Bruland 2012), and the Cd and Ni concentration profiles of non-TMC samples match those of TMC samples very well (Fig. 3), indicating that Cd and Ni are not contaminated using the regular CTD rosette and Niskin bottles. For the RR1804 seawater samples, the lowest Cd concentration of surface seawater is 0.00 nmol L^{-1} (below the detection limit, see Table 1) and the lowest Ni concentration of surface seawater is 2.31 nmol L^{-1} (Table 2), both are similar to Cd and Ni

concentrations of the oligotrophic surface seawater and again indicate that Cd and Ni are not contaminated. For RR1804 samples, there are 6 Ni data points deviating from the main trendline of the Ni profile at a sigma-theta of ~ 26.5 , which might reflect the Ni-related redox processes. However, a recent study showed that Ni is not influenced by redox processes in the ETNP ODZ (Yang et al. 2021). Therefore, these Ni concentration outliers most likely result from contamination of Ni during sampling and/or analysis. We chose to present these outliers to better reflect the cleanliness of the regular CTD rosette sampling.

The Mn profiles from RR1804 show relatively high Mn concentrations in surface waters, a Mn maximum in the subsurface

Table 2. The maximum (Max), minimum (Min), and median values of trace metals of RR1804 and RR1805 samples.

	Cd nmol L^{-1}	Ni nmol L^{-1}	Mn nmol L^{-1}	Ce pmol L^{-1}	Fe nmol L^{-1}	Zn nmol L^{-1}	Cu nmol L^{-1}	Pb pmol L^{-1}
RR1804 Min	0.00	2.31	0.21	0.6	0.61	0.50	0.69	2.5
RR1804 Max	1.20	13.23	7.73	14.8	129.85	107.43	345.30	145.1
RR1804 Median	0.79	5.41	2.49	6.2	1.96	8.04	1.14	24.0
RR1805 Min	0.01	2.80	1.22	—	0.06	0.04	0.65	7.9
RR1805 Max	1.03	8.40	12.01	—	6.52	3.75	3.04	101.3
RR1805 Median	0.70	4.84	4.87	—	1.00	0.49	1.06	16.1

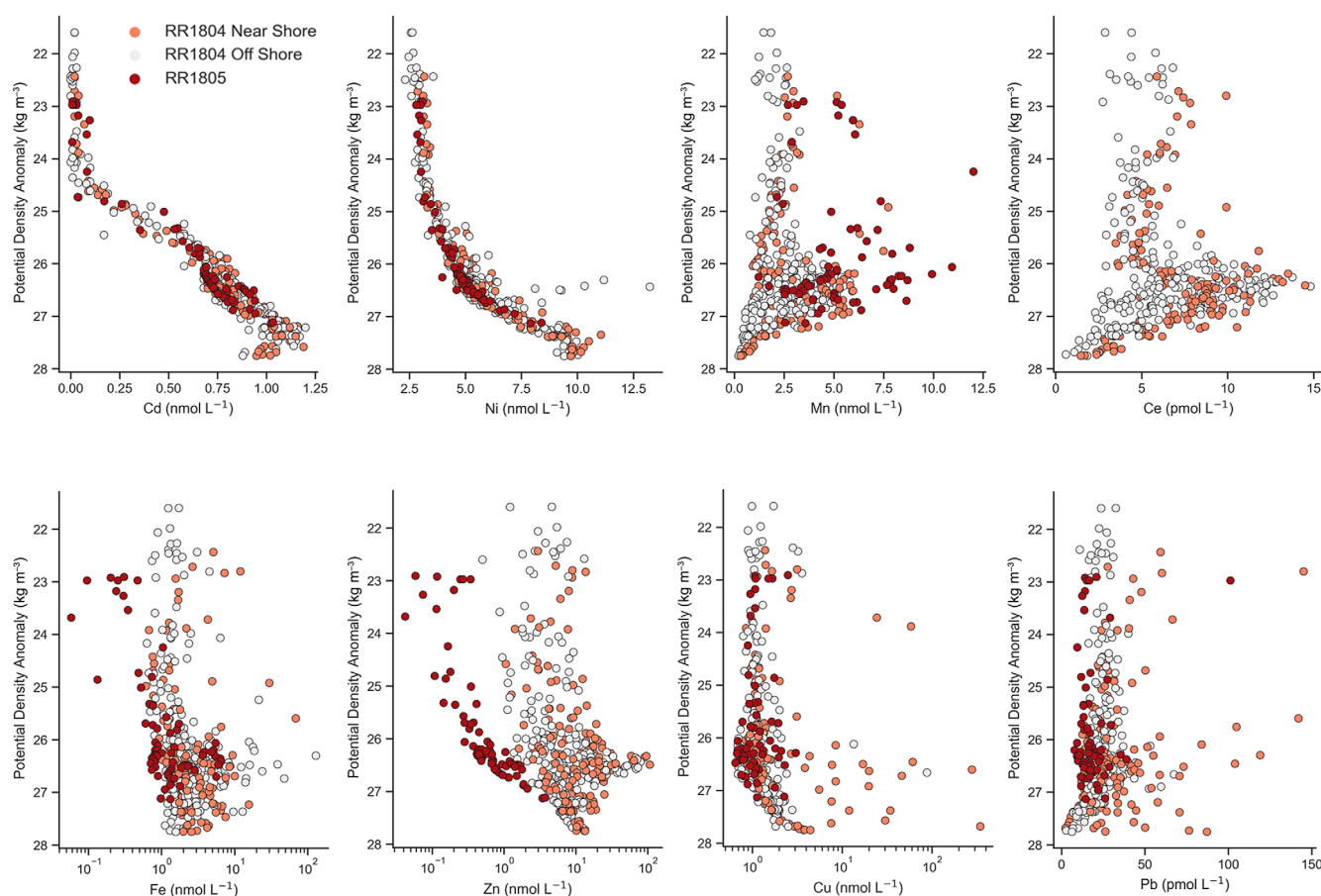


Fig. 3. Trace metal concentrations compared between samples taken on the RR1804 cruise using a non-TMC sampling system, and those from the RR1805 cruise, where a TMC sampling system was employed. Note that the concentrations of Fe, Zn, and Cu are shown on a logarithmic scale. RR1804 samples were split into near-shore (light red circles) and offshore (light gray circles) samples. RR1805 samples were shown as dark red circles. See Fig. 1 for the information of near-shore and offshore stations.

seawater (at a sigma-theta of ~ 26.3), and the lowest Mn in deep water where the Mn concentration can be as low as 0.21 nmol L^{-1} (Fig. 3; Table 2). The Mn profiles of the RR1805 stations are very similar to the RR1804 profiles, especially those from the RR1804 near-shore stations (Fig. 3). However, it is worth noting that seawater samples from the RR1805 cruise have even higher Mn concentrations than RR1804 samples (Fig. 3; Table 2), which we attribute to Stas. P1 to P4 being closer to the shelf. Overall, the similarity between RR1804 and RR1805 samples, and the extreme depletion of Mn in deep water, show that Mn-clean samples can be collected using the non-TMC sampling system. The profiles of Ce are very similar to those of Mn. Data on LREEs are not available for RR1805, but the lowest Ce concentration of RR1804 samples is 0.6 pmol L^{-1} , indicating that Ce and other LREEs (La, Pr, and Nd) can also be sampled cleanly using the regular CTD rosette.

Fe, Zn, Cu, and Pb appear to be contaminated using the regular CTD rosette, based on a comparison between RR1804 and RR1805 data. Fe and Zn are obviously contaminated. Both the lowest and highest Fe and Zn concentrations of RR1804

samples are much higher than those of RR1805 samples (Fig. 3; Table 2). The highest Fe ($129.85 \text{ nmol L}^{-1}$) and Zn ($107.43 \text{ nmol L}^{-1}$) concentrations of RR1804 samples are much higher than typically reported for the global ocean (Schlitzer et al. 2018). Even the median value of the RR1804 Fe concentrations is higher than typical open ocean seawater; the median value of RR1804 Zn is similar to the deep ocean Zn concentration (Table 2) (Schlitzer et al. 2018). Cu is less obviously contaminated, with many of the RR1804 samples having concentrations similar to RR1805 samples. However, there is clearly at least sporadic contamination, with some RR1804 samples having Cu concentrations above 10 nmol L^{-1} , which is not consistent with oceanographic observations (Schlitzer et al. 2018). Finally, the case for Pb contamination during sampling is the most ambiguous, with most of the RR1804 samples having concentrations slightly higher than RR1805 samples; however, there is clearly at least sporadic contamination, with some RR1804 samples having Pb concentrations much higher than RR1805 samples above 100 pmol L^{-1} . Moreover, the repeatability of Pb concentrations between the samples collected at the

same station at different times (Stas. 19 and 23, and Stas. 9 and 28) is poor (Fig. 1), indicating that Pb can be contaminated using ship's regular sampling systems.

Our results show that the ship's regular sampling system is clean for Cd, Ni, Mn, and LREEs. However, in this study, several factors limited our assessment of the cleanliness of the ship's regular sampling system, including a lack of the intercomparison between the TMC sampling and non TMC sampling from crossover stations and replicate analysis by other labs. Although our results show it is feasible to use non TMC sampling system to study Cd, Ni, Mn, and LREEs, we suggest that we should be conservative about this approach and a stricter intercomparison be carried out in the near future.

Cd in the ETNP ODZ

The distribution of Cd is similar on both the zonal and meridional sections of the RR1804 cruise. Dissolved Cd (dCd) concentrations are extremely low in surface seawater and increase with depth (Figs. 3, 4). Around the halocline and oxycline, dCd increases rapidly from surface to subsurface waters.

The Cd* of surface seawater is about $-0.05 \text{ nmol L}^{-1}$ in the ETNP. Considering that Cd is extremely depleted in surface seawater, this simply reflects near-quantitative biological uptake of both Cd and phosphate. There is a negative excursion of Cd* around the oxycline at the sigma-theta of $\sim 25 \text{ kg m}^{-3}$, where the Cd* can be as low as $\sim -0.40 \text{ nmol L}^{-1}$. Below the oxycline, Cd* increases with depth (Figs. 4, 5).

Among all the water masses in the ETNP ODZ, 13CW has the lowest oxygen concentration (less than $1 \mu\text{mol kg}^{-1}$) and serves as the best candidate to study the CdS hypothesis. 13CW is characterized by a low oxygen concentration ($< 1 \mu\text{mol kg}^{-1}$) and a high salinity ($\sim 34.8 \text{ psu}$), so both oxygen and salinity sections were plotted to help identify it (Fig. 4). The average Cd* of 13CW is $-0.06 \pm 0.06 \text{ nmol L}^{-1}$ (2SD, $n = 30$) and its average dissolved oxygen concentration is $0.79 \pm 0.42 \mu\text{mol kg}^{-1}$. The average Cd* of water samples with oxygen concentrations less than $1 \mu\text{mol kg}^{-1}$ is $-0.11 \pm 0.14 \text{ nmol L}^{-1}$ (2SD, $n = 137$). These average values are not distinguishable from the Cd* of oxic surface waters, which is about $-0.05 \text{ nmol L}^{-1}$ (Fig. 5), indicating no obvious loss of Cd compared to phosphate in the oxygen-deficient seawater in the ETNP.

Prevalent negative Cd* values are observed around the oxycline (also halocline) above the ODZ in the ETNP (Figs. 4, 5). Negative Cd* values can result from several potential mechanisms, such as (1) a higher Cd:PO₄³⁻ export ratio (i.e., preferential uptake of Cd relative to phosphate) in surface seawater (Löscher et al. 1998; Elderfield and Rickaby 2000; Cullen 2006); (2) a deeper remineralization of Cd than PO₄³⁻ (Wu and Roshan 2015); and (3) CdS precipitation (Janssen et al. 2014). Near the oxycline, some of the very negative Cd*

values ($< -0.25 \text{ nmol L}^{-1}$) seem to be related to the Pacific Subarctic Upper Water (Fig. 5). These negative Cd* values may be related to the preformed Cd* of surface waters in the high-nutrient, low-chlorophyll subarctic North Pacific, where preferential uptake of Cd relative to phosphate has been observed (Löscher et al. 1998; Cullen 2006; Janssen et al. 2017). There are a few samples with extremely low Cd* values (around $-0.40 \text{ nmol L}^{-1}$). These low Cd* values cannot be explained by the preformed Cd* signature alone, and they may result from the preferential remineralization of PO₄³⁻ compared to Cd above the ODZ. This is consistent with previous studies showing that the more labile portion of bound P is remineralized faster than Cd at shallow depths in the euphotic zone (Bourne et al. 2018).

The Cd* minimum is also associated with the oxycline in the open tropical South Pacific (John et al. 2018; Sieber et al. 2019; de Souza et al. 2022). Our data confirmed this feature in the ETNP. Thus, the Cd* minimum is associated with the oxycline throughout the tropics; the explanation of this feature remains a mystery but may be attributable to the presence of heterotrophic prokaryotes and low-light-adapted autotrophic prokaryotes (Ohnemus et al. 2019; de Souza et al. 2022). Future work is required to fully understand the mechanism(s) of the tropical Cd loss, particularly by combining trace metal studies with microbial biological studies through 'omics approaches, as has been suggested by de Souza et al. (2022).

Although the ETNP ODZ seems to be a promising region to seek confirmation of the CdS hypothesis, due to the extreme depletion of oxygen in this region, we do not find that Cd is depleted relative to phosphate within the most oxygen-deficient ($[\text{O}_2] < 1 \mu\text{mol kg}^{-1}$) waters, and thus we do not find evidence to support precipitation of CdS within ODZs. Our work joins a growing body of literature suggesting that CdS precipitation does not greatly impact Cd distribution in the oceans (John et al. 2018; Yang et al. 2018; de Souza et al. 2022).

Manganese cycling in the ETNP ODZ

Depth profiles of dissolved Mn in the ocean typically display surface enrichments attributable to external input sources (primarily aerosol deposition and riverine input), and a relative depletion of Mn at depth due to scavenging (Landing and Bruland 1980; Shiller 1997; Boyle et al. 2005). Although we did observe a surface enrichment of Mn in the ETNP, this enrichment is small compared to the subsurface maximum of Mn within the ODZ (Fig. 6a,e).

For the zonal section of Mn, extending westward from near the continental margin into the North Pacific, the subsurface Mn plume exhibits a wedge shape (Fig. 6a). At Sta. 30 near the coast, high Mn concentrations extend throughout the water column from 100 to 800 m depth. Moving offshore, further away from the coast, less and less high-Mn seawater is observed at depth. At Sta. 22, the most offshore station, high-

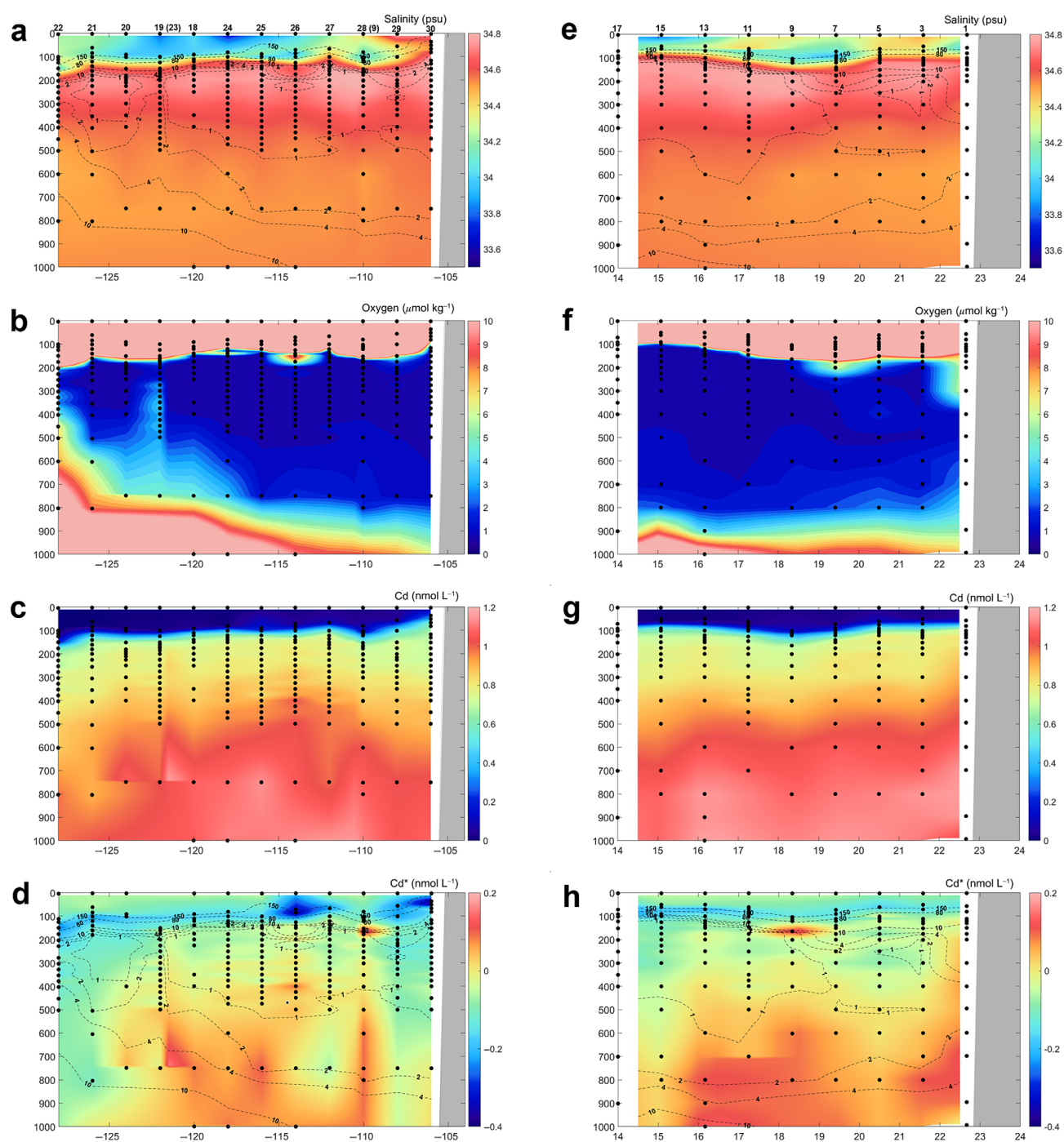


Fig. 4. The zonal (left column) and meridional (right column) sections of salinity, oxygen, Cd, and Cd* in the ENTp ODZ. Gray regions indicate the continental shelf/slope regions. Station IDs are labeled above the salinity section plots. Salinity (**a,e**) and Cd* (**d,h**) sections are overlaid with dashed contours of dissolved oxygen with contour levels of 1, 2, 4, 10, 80, and 150 $\mu\text{mol kg}^{-1}$ labeled.

Mn seawater is confined to ~ 200 m depth. The distribution of low-oxygen seawater ($< 4 \mu\text{mol kg}^{-1}$ $[\text{O}_2]$) along this same zonal section exhibits a similar wedge shape to Mn (Fig. 6a), such that low oxygen concentrations correspond to high Mn concentrations, and vice versa.

Mn is released from sediments during early diagenesis (Froelich et al. 1979; Sundby et al. 1986), as are other metals including Fe, Co, and Ce (Bruland and Lohan 2003; Noble et al. 2012; Morton et al. 2019), and sedimentary release is the likely source of Mn in the subsurface plume. In the ETNP, the

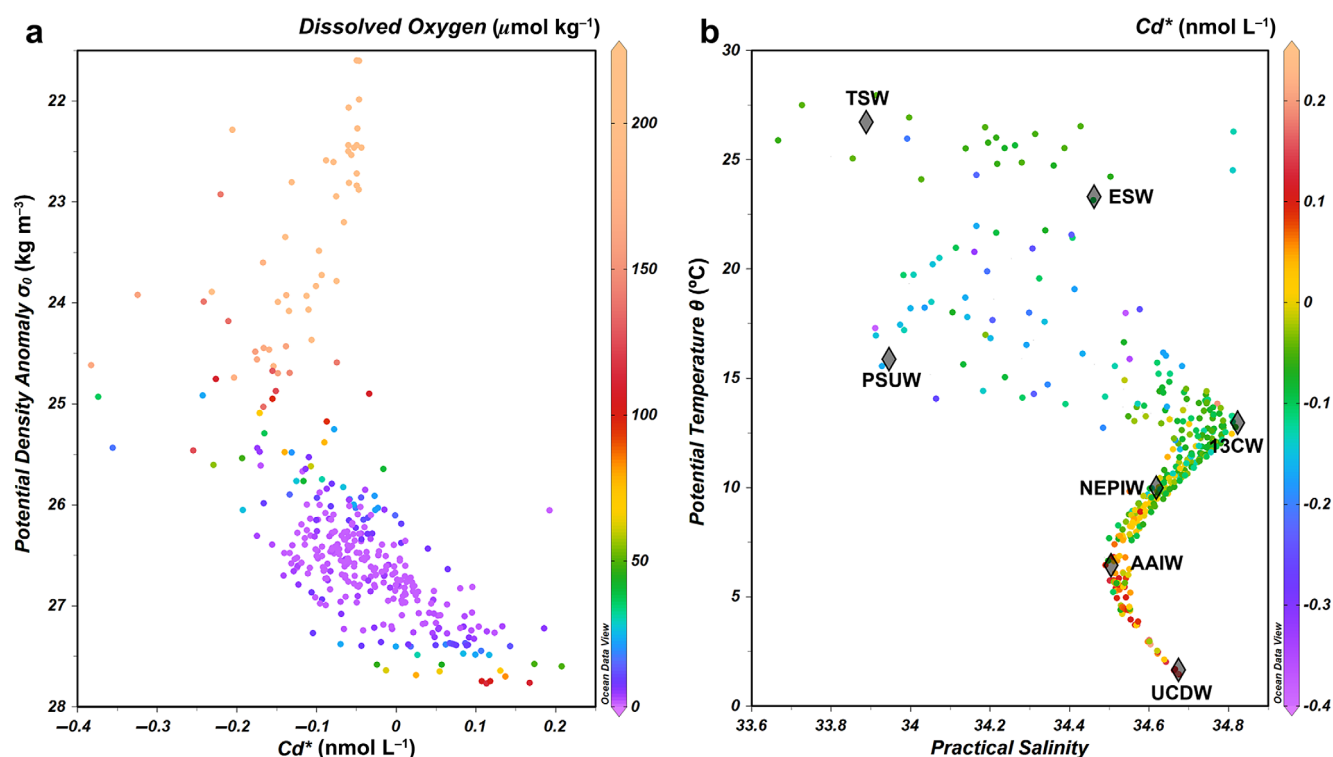


Fig. 5. The Cd* values of RR1804 samples. Colors reflect oxygen concentrations (a) and Cd* values (b).

California Undercurrent flows poleward near the continental shelf, generating mesoscale subsurface eddies that transport 13CW water westwards (Evans et al. 2020) to facilitate the off-shore transportation of Mn and other trace metals.

There is an overall pattern of decreasing Mn away from the continental margin, but there are three hotspots with higher Mn concentrations observable in the zonal section, centered at roughly 125°W, 118°W, and 112°W (Fig. 6a). Each of these locations also has a high percentage of 13CW based on a water mass analysis of this zonal transect (Evans et al. 2020). Among them, the hotspot at Sta. 28 near 112°W has the highest percentage of 13CW (80–100%), whereas the percentages of 13CW in the other two hotspots are between 60% to 80%. This likely explains why the high-Mn hotspot near 112°W has a higher Mn concentration. Regions of high Mn concentrations are also generally coincident with the secondary nitrite maxima and elevated iodide concentrations (Fig. 6b,c). The nitrite enrichment is often attributed to the active microbial nitrogen cycle processes. Elevated iodide concentrations, in particular those exceeding the average total inorganic iodine amount (470 nmol L⁻¹) in the ocean (i.e., excess iodine) (Luther III et al. 1995), not only reflect in situ iodate reduction, but also are derived from the lateral advection of iodide from reducing shelf sediments (Farenkopf and Luther 2002; Cutter et al. 2018; Moriyasu et al. 2020). This indicates that Mn and iodide share the same sedimentary source, and both the overall pattern of high Mn concentrations between roughly 100 and 400 m depth, as well as the higher Mn concentrations in

“hotspots” can be attributed to the westward transportation of 13CW by subsurface eddies (Fig. 7), although the importance of in situ microbial redox processes cannot be neglected.

Oxygen concentrations appear to be a key control on the concentration of Mn in the ETNP ODZ. High Mn concentrations (> 2 nmol L⁻¹) are only observed where dissolved oxygen concentrations are less than 4 μmol kg⁻¹ (Fig. 6a,e). At Sta. 19, seawater with an oxygen concentration of ~ 4 μmol kg⁻¹ intrudes upwards into the overlying low-oxygen seawater, which is consistent with the upwelling of NEPIW into 13CW (Evans et al. 2020). Waters with a higher oxygen concentration and higher NEPIW percentage also have distinctly lower Mn concentrations. The increase in oxygen is modest (from < 1 to 4 μmol kg⁻¹). However, it appears that Mn is so sensitive to oxygen that it can be influenced by even small increases in oxygen concentration. Besides oxygen concentrations, 13CW and NEPIW also have different water mass sources, different trajectories that transport them to the ETNP ODZ, and different interactions with the shelf within the ODZ. All these factors could result in the difference in their Mn concentrations.

The insight provided by the zonal section makes it easier to interpret observations on the meridional section. Subsurface Mn maxima are also observed on the meridional section, characterized by two hotspots, one near Sta. 9 centered at roughly 18°N and the other one near Sta. 3 centered at roughly 22°N (Fig. 6e). The hotspot at Sta. 9 is the same hotspot as observed at Sta. 28 in the zonal section (Fig. 6a,e), suggesting that both hotspots on the meridional section likely originate from

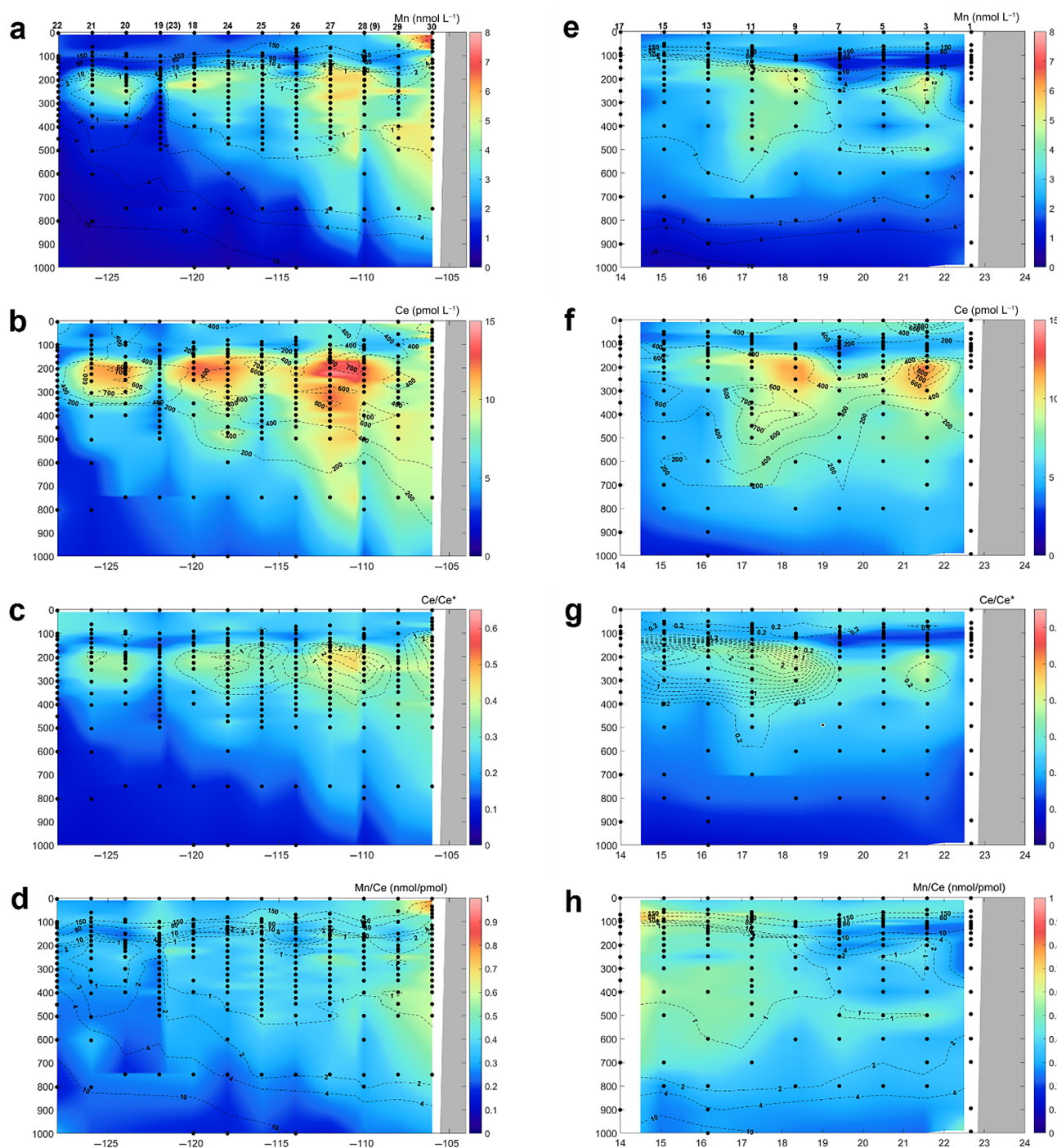


Fig. 6. Zonal (left column) and meridional (right column) sections of Mn, Ce, Ce anomaly, and Mn/Ce in the ENTP ODZ. Gray regions indicate the continental shelf/slope regions. Station IDs are labeled above the Mn section plots. Mn sections (**a,e**) are overlaid with dashed contours of dissolved oxygen with contour levels of 1, 2, 4, 10, 80, and 150 $\mu\text{mol kg}^{-1}$ labeled. Ce sections (**b,f**) are overlaid with dashed contours of iodide with contour levels of 200, 400, 600, 700, and 800 nmol L^{-1} labeled. Ce anomaly sections (**c,g**) are overlaid with dashed contours of nitrite with contour levels of 0.2, 1, and 2 $\mu\text{mol L}^{-1}$ labeled. Mn/Ce sections (**d,h**) are overlaid with dashed contours of dissolved oxygen with contour levels of 1, 2, 4, 10, 80, and 150 $\mu\text{mol kg}^{-1}$ labeled.

continental shelf input. Above the Mn hotspot at Sta. 3, there is a low Mn region around 100–150 m from Stas. 1 to 7. This low Mn region seems to be related to the 13CW water mass based on the salinity (Figs. 4e, 6e), but is associated with

oxygen concentrations higher than 4 $\mu\text{mol kg}^{-1}$ (Fig. 6e). This indicates that the low Mn region is formed by removing the oxygen-sensitive Mn that originates from the continental shelf input.

Ce cycling in the ETNP ODZ

In the ETNP, Ce and Ce anomaly are highly correlated with Mn concentrations (Fig. 7), and sections of Mn, Ce, and Ce anomaly are quite similar (Fig. 6a–c,e–g). A high correlation

between Mn and Ce has also been observed in other regions, such as the Cariaco Trench (de Baar et al. 1988), off the African shelf (Zheng et al. 2016), and in the Arabian Sea (Floback and Moffett 2021). In the zonal section, the Ce anomaly

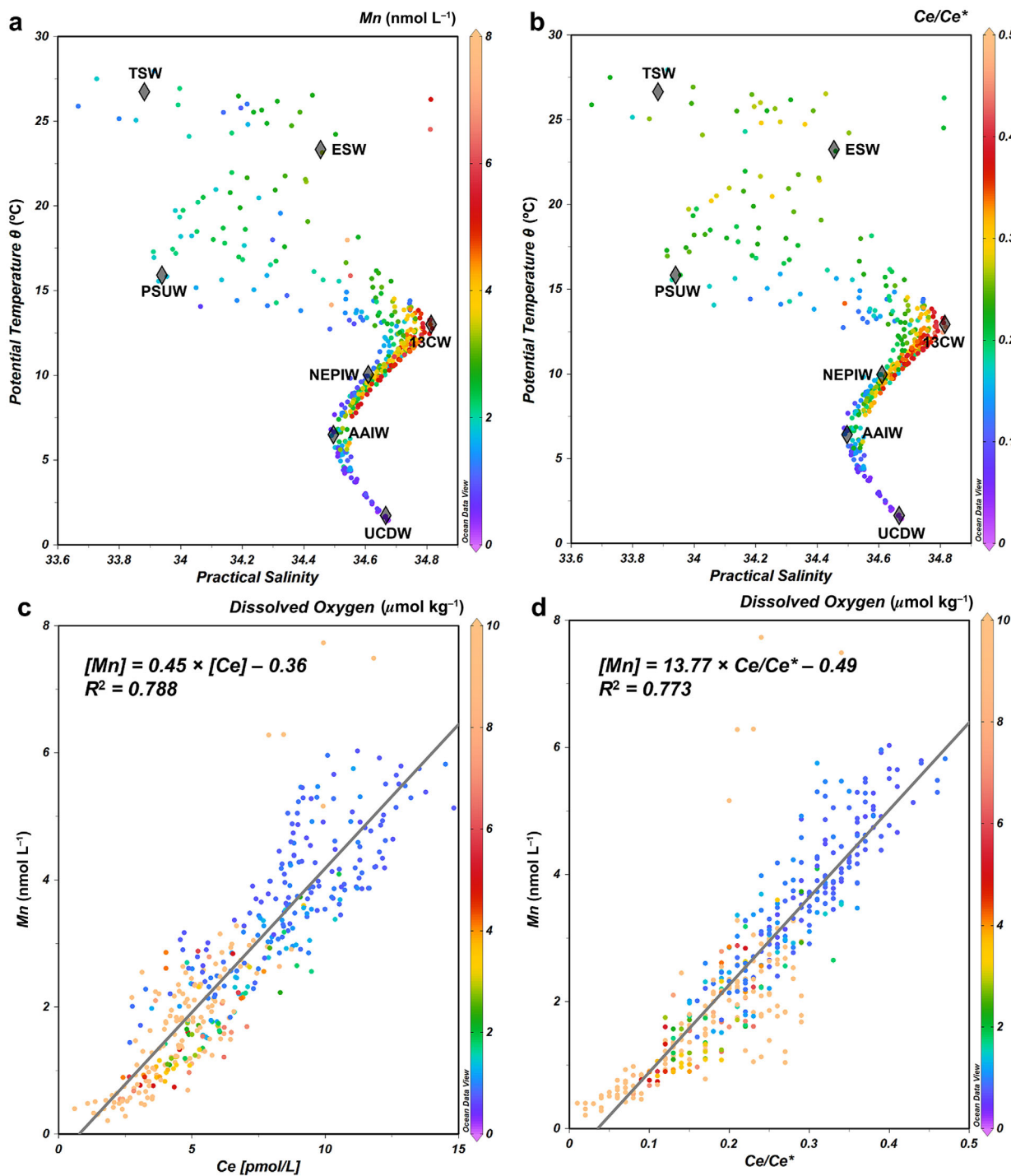


Fig. 7. (a,b) T–S diagrams of the water samples in this study with colors showing Mn concentrations and Ce anomaly values. (c,d) The correlations between Mn and Ce, and Mn and Ce anomaly are shown by gray lines representing linear regressions, as described by the equations and R^2 values shown on each plot. Colors indicate seawater oxygen concentrations.

values in the subsurface Ce plume are higher than surface Ce anomaly values (Fig. 6b,c), probably indicating that surface and subsurface Ce have different sources and/or undergo different degrees of in situ redox processes. Considering the correlation between Ce and Mn, we assume that shelf input probably is also the main source of subsurface Ce. Eolian and riverine input are likely the main sources of surface Ce and they are characterized by a weak or the absence of Ce depletion relative to the neighboring REEs (Goldstein and Jacobsen 1988; Greaves et al. 1994). Photoreduction of manganese oxides in surface seawater may also contribute to the supply of Ce to surface seawater (Sunda et al. 1983).

Although there is an overall similarity between Mn and Ce in the ETNP ODZ, there are still some noteworthy differences between the two. Mn concentrations decrease abruptly when oxygen concentrations are above $4 \mu\text{mol kg}^{-1}$, while relatively high Ce concentrations can still be observed in the regions where oxygen concentrations are higher than $4 \mu\text{mol kg}^{-1}$ and Mn is depleted (Fig. 6a,b,e,f), suggesting differences in their removal from seawater in the presence of oxygen. The observation here is consistent with previous studies showing that microbial Mn oxidation is three times faster than microbial Ce oxidation (Moffett 1990). This pattern is also observed in Mn/Ce ratios. In the zonal section of Mn/Ce, high Mn/Ce ratios are observed near the coast and lower Mn/Ce ratios are observed at higher oxygen concentrations (Fig. 6d), indicating that Mn is removed from seawater more rapidly than Ce when oxygen concentrations increase in the ODZ seawater. In the meridional section of Mn/Ce, a striking feature is that in the ODZ, almost all the regions with high Mn/Ce ratios ($> 0.5 \text{ nmol/pmole}$) are associated with oxygen concentrations less than $1 \mu\text{mol kg}^{-1}$ (Fig. 6h). The Mn/Ce ratios of the lowest-oxygen seawater ($< 1 \mu\text{mol kg}^{-1}$) in the meridional section are similar to the shelf Mn/Ce ratio in the zonal section, indicating that Mn and Ce in the low-oxygen seawater originate at the continental shelf.

Finally, we note that the Mn and Ce hotspot at roughly 18°N , 110°W (Fig. 6) is next to Socorro Island, where a series of underwater eruptions occurred at 210 m depth on its west flank in 1993 (Siebe et al. 1995). Hydrothermal waters are usually characterized by elevated Mn and REE concentrations, and the absence of a Ce anomaly (i.e., $\text{Ce/Ce}^* = 1$) (Douville et al. 1999; Resing et al. 2015). Although suspended particles or dissolved metals from the underwater eruptions would have been advected away long ago, diagenesis of reduced materials deposited on the island's flanks may continue to supply material to the water column. Therefore, it is possible that the volcanic features of Mn and Ce from the underwater eruptions three decades ago are still partially preserved here.

Conclusions

Our new results presented here, combined with the distribution of iodine species (Moriyasu et al. 2020) and water mass analysis (Evans et al. 2020), suggest that lateral inputs of

various elements within the ODZ are important throughout the ETNP. Elevated plumes of Mn and Ce are associated with a discrete water mass (13CW) and with subsurface eddies that transport materials offshore within the 13CW. "Hotspots" with elevated concentrations of Mn, Ce, and iodine were observed on both transects and each was associated with high percentages of 13CW water. The origin of the enrichments within the hotspots cannot be determined conclusively, but the co-variation with excess iodine suggests that they originate from benthic inputs at continental margins.

Shelf-released Mn is extremely sensitive to oxygen, such that dissolved Mn appears to be quickly removed from ODZ seawater when dissolved oxygen concentrations increase to $\sim 4 \mu\text{mol kg}^{-1}$. The concentrations of Ce are also lower in ODZ seawater at higher $[\text{O}_2]$, though Ce appears to be less quickly lost when small amounts of oxygen ($> \sim 4 \mu\text{mol kg}^{-1}$) are present.

We do not find that Cd is depleted relative to phosphate within the most oxygen-deficient ($[\text{O}_2] < 1 \mu\text{mol kg}^{-1}$) waters of the ETNP ODZ, and thus we do not find evidence to support precipitation of CdS within ODZs. Low Cd* values are observed in the ETNP around the oxycline, which may be related to the preformed Cd* signal of seawater originating from the subarctic North Pacific, and the preferential remineralization of PO_4^{3-} compared to Cd above the ODZ. Future studies are required to fully understand the mechanisms of the Cd loss in the oxycline throughout the tropics.

This study employed a non-TMC sampling system, the ship's regular CTD rosette and Niskin bottles, to collect two high-resolution sections of metal distribution. We found that this approach provided samples which were clean for Cd, Ni, Mn, and LREEs, though not for Fe, Zn, Cu, and Pb. This is potentially valuable because it greatly expands the prospects for studies of these elements when a TMC sampling technique is unavailable. Despite the encouraging results here, we suggest that we should be conservative about using non-TMC sampling technique to study trace metals before more and stricter evaluation of it.

Data availability statement

All data generated for this study can be found in the Biological and Chemical Oceanography Data Management Office (BCO-DMO). The hydrographic and nutrient data of RR1804-RR1805 are available via <http://lod.bco-dmo.org/id/dataset/779185>. The iodine speciation data are available via <https://www.bco-dmo.org/dataset/776552>. Trace metal data are available via <http://lod.bco-dmo.org/id/dataset/872434>.

References

- Billler, D. V., and K. W. Bruland. 2012. Analysis of Mn, Fe, Co, Ni, Cu, Zn, Cd, and Pb in seawater using the Nobias-chelate PA1 resin and magnetic sector inductively coupled plasma mass spectrometry (ICP-MS). *Mar. Chem.* **130–131**: 12–20. doi:10.1016/j.marchem.2011.12.001

- Bourne, H. L., J. K. B. Bishop, P. J. Lam, and D. C. Ohnemus. 2018. Global spatial and temporal variation of Cd:P in euphotic zone particulates. *Global Biogeochem. Cycl.* **32**: 1123–1141. doi:[10.1029/2017GB005842](https://doi.org/10.1029/2017GB005842)
- Boyle, E. A. 1988. Cadmium: Chemical tracer of deepwater paleoceanography. *Paleoceanography* **3**: 471–489.
- Boyle, E. A., B. A. Bergquist, R. A. Kayser, and N. Mahowald. 2005. Iron, manganese, and lead at Hawaii Ocean time-series station ALOHA: Temporal variability and an intermediate water hydrothermal plume. *Geochim. Cosmochim. Acta* **69**: 933–952. doi:[10.1016/j.gca.2004.07.034](https://doi.org/10.1016/j.gca.2004.07.034)
- Brandes, J. A., A. H. Devol, T. Yoshinari, D. A. Jayakumar, and S. W. A. Naqvi. 1998. Isotopic composition of nitrate in the central Arabian Sea and eastern tropical North Pacific: A tracer for mixing and nitrogen cycles. *Limnol. Oceanogr.* **43**: 1680–1689. doi:[10.4319/lo.1998.43.7.1680](https://doi.org/10.4319/lo.1998.43.7.1680)
- Bruland, K. W. 1980. Oceanographic distributions of cadmium, zinc, nickel, and copper in the North Pacific. *Earth Planet. Sci. Lett.* **47**: 176–198.
- Bruland, K. W., and M. C. Lohan. 2003. Controls of trace metals in seawater, p. 625. *In* Treatise on geochemistry, v. **6**. Pergamon.
- Bruland, K. W., E. L. Rue, G. J. Smith, and G. R. DiTullio. 2005. Iron, macronutrients and diatom blooms in the Peru upwelling regime: Brown and blue waters of Peru. *Mar. Chem.* **93**: 81–103. doi:[10.1016/j.marchem.2004.06.011](https://doi.org/10.1016/j.marchem.2004.06.011)
- Canfield, D. E., F. J. Stewart, B. Thamdrup, L. De Brabandere, T. Dalsgaard, E. F. Delong, N. P. Revsbech, and O. Ulloa. 2010. A cryptic sulfur cycle in oxygen-minimum-zone waters off the Chilean coast. *Science* **330**: 1375–1378. doi:[10.1126/science.1196889](https://doi.org/10.1126/science.1196889)
- Chang, B. X., A. H. Devo, and S. R. Emerson. 2012. Fixed nitrogen loss from the eastern tropical North Pacific and Arabian Sea oxygen deficient zones determined from measurements of N₂:Ar. *Global Biogeochem. Cycl.* **26**: 1–8. doi:[10.1029/2011GB004207](https://doi.org/10.1029/2011GB004207)
- Conway, T. M., and S. G. John. 2015a. Biogeochemical cycling of cadmium isotopes along a high-resolution section through the North Atlantic Ocean. *Geochim. Cosmochim. Acta* **148**: 269–283. doi:[10.1016/j.gca.2014.09.032](https://doi.org/10.1016/j.gca.2014.09.032)
- Conway, T. M., and S. G. John. 2015b. The cycling of iron, zinc and cadmium in the North East Pacific Ocean—Insights from stable isotopes. *Geochim. Cosmochim. Acta* **164**: 262–283. doi:[10.1016/j.gca.2015.05.023](https://doi.org/10.1016/j.gca.2015.05.023)
- Cullen, J. T. 2006. On the nonlinear relationship between dissolved cadmium and phosphate in the modern global ocean: Could chronic iron limitation of phytoplankton growth cause the kink? *Limnol. Oceanogr.* **51**: 1369–1380. doi:[10.4319/lo.2006.51.3.1369](https://doi.org/10.4319/lo.2006.51.3.1369)
- Cutter, G. A., and K. W. Bruland. 2012. Rapid and non-contaminating sampling system for trace elements in global ocean surveys. *Limnol. Oceanogr. Methods* **10**: 425–436. doi:[10.4319/lom.2012.10.425](https://doi.org/10.4319/lom.2012.10.425)
- Cutter, G. A., J. G. Moffett, M. C. Nielsdóttir, and V. Sanial. 2018. Multiple oxidation state trace elements in suboxic waters off Peru: In situ redox processes and advective/diffusive horizontal transport. *Mar. Chem.* **201**: 77–89. doi:[10.1016/j.marchem.2018.01.003](https://doi.org/10.1016/j.marchem.2018.01.003)
- Cutter, G. A., K. Casciotti, P. Croot, W. Geibert, L.-E. Heimbürger, M. C. Lohan, H. Planquette, and T. van de Fliedt. 2017. Sampling and sample-handling protocols for GEOTRACES Cruises, Version 3.0. GEOTRACES Standards and Intercalibration Committee.
- de Baar, H. J. W., C. R. German, H. Elderfield, and P. Van Gaans. 1988. Rare earth element distributions in anoxic waters of the Cariaco Trench. *Geochim. Cosmochim. Acta* **52**: 1203–1219.
- De Baar, H. J. W., K. R. Timmermans, P. Laan, H. H. De Porto, and S. Ober. 2008. Titan: A new facility for ultraclean sampling of trace elements and isotopes in the deep oceans in the international Geotraces program. **111**: 4–21. doi:[10.1016/j.marchem.2007.07.009](https://doi.org/10.1016/j.marchem.2007.07.009)
- de Souza, G. F., D. Vance, M. Sieber, T. M. Conway, and S. H. Little. 2022. Re-assessing the influence of particle-hosted sulphide precipitation on the marine cadmium cycle. *Geochim. Cosmochim. Acta* **322**: 274–296. doi:[10.1016/j.gca.2022.02.009](https://doi.org/10.1016/j.gca.2022.02.009)
- Douville, E., P. Bienvenu, J.-L. Charlou, J.-P. Donval, Y. Fouquet, P. Appriou, and T. Gamo. 1999. Yttrium and rare earth elements in fluids from various deep-sea hydrothermal systems—Evidence for heat extraction from magma chambers or cracking fronts? *Geochimica Cosmochim. Acta Theriol.* **63**: 627–643.
- Elderfield, H., and R. E. M. Rickaby. 2000. Oceanic Cd/P ratio and nutrient utilization in the glacial Southern Ocean. *Nature* **405**: 305–310. doi:[10.1038/35012507](https://doi.org/10.1038/35012507)
- Evans, N., and others. 2020. The role of water masses in shaping the distribution of redox active compounds in the Eastern Tropical North Pacific oxygen deficient zone and influencing low oxygen concentrations in the eastern Pacific Ocean. *Limnol. Oceanogr.* **65**: 1688–1705. doi:[10.1002/lno.11412](https://doi.org/10.1002/lno.11412)
- Farrenkopf, A. M., and G. W. Luther. 2002. Iodine chemistry reflects productivity and denitrification in the Arabian Sea: Evidence for flux of dissolved species from sediments of western India into the OMZ. *Deep Res. Part II Top. Stud. Oceanogr.* **49**: 2303–2318. doi:[10.1016/S0967-0645\(02\)00038-3](https://doi.org/10.1016/S0967-0645(02)00038-3)
- Fiedler, P. C., and L. D. Talley. 2006. Hydrography of the eastern tropical Pacific: A review. *Prog. Oceanogr.* **69**: 143–180. doi:[10.1016/j.pocean.2006.03.008](https://doi.org/10.1016/j.pocean.2006.03.008)
- Floback, A. E., and J. W. Moffett. 2021. Rare earth element distributions in the Arabian Sea reveal the influence of redox processes within the oxygen deficient zone. *Chem. Geol.* **577**: 120214. doi:[10.1016/j.chemgeo.2021.120214](https://doi.org/10.1016/j.chemgeo.2021.120214)
- Froelich, P. N., and others. 1979. Early oxidation of organic matter in pelagic sediments of the eastern equatorial

- Atlantic: Suboxic diagenesis. *Geochim. Cosmochim. Acta* **43**: 1075–1090. doi:[10.1016/0016-7037\(79\)90095-4](https://doi.org/10.1016/0016-7037(79)90095-4)
- Fuchsman, C. A., A. H. Devol, K. L. Casciotti, C. Buchwald, B. X. Chang, and R. E. A. Horak. 2018. An N isotopic mass balance of the Eastern Tropical North Pacific oxygen deficient zone. *Deep Res. Part II Top. Stud. Oceanogr.* **156**: 137–147. doi:[10.1016/j.dsr2.2017.12.013](https://doi.org/10.1016/j.dsr2.2017.12.013)
- Goldstein, S. J., and S. B. Jacobsen. 1988. Rare earth elements in river waters. *Earth Planet. Sci. Lett.* **89**: 35–47. doi:[10.1016/0012-821X\(88\)90031-3](https://doi.org/10.1016/0012-821X(88)90031-3)
- Greaves, M. J., P. J. Statham, and H. Elderfield. 1994. Rare earth element mobilization from marine atmospheric dust into seawater. *Mar. Chem.* **46**: 255–260. doi:[10.1016/0304-4203\(94\)90081-7](https://doi.org/10.1016/0304-4203(94)90081-7)
- Hatje, V., K. W. Bruland, and A. R. Flegal. 2014. Determination of rare earth elements after pre-concentration using NOBIAS-chelate PA-1[®] resin: Method development and application in the San Francisco Bay plume. *Mar. Chem.* **160**: 34–41. doi:[10.1016/j.marchem.2014.01.006](https://doi.org/10.1016/j.marchem.2014.01.006)
- Hawco, N. J., and others. 2020. Metal isotope signatures from lava-seawater interaction during the 2018 eruption of Kīlauea. *Geochim. Cosmochim. Acta* **282**: 340–356. doi:[10.1016/j.gca.2020.05.005](https://doi.org/10.1016/j.gca.2020.05.005)
- Hawco, N. J., D. C. Ohnemus, J. A. Resing, B. S. Twining, and M. A. Saito. 2016. A dissolved cobalt plume in the oxygen minimum zone of the eastern tropical South Pacific. *Biogeosciences* **13**: 5697–5717. doi:[10.5194/bg-13-5697-2016](https://doi.org/10.5194/bg-13-5697-2016)
- Huang, H., M. Gutjahr, G. Kuhn, E. C. Hathorne, and A. Eisenhauer. 2021. Efficient extraction of past seawater Pb and Nd isotope signatures from Southern Ocean sediments. *Geochem. Geophys. Geosyst.* **22**: 1–22. doi:[10.1029/2020GC009287](https://doi.org/10.1029/2020GC009287)
- Janssen, D. J., T. M. Conway, S. G. John, J. R. Christian, D. I. Kramer, T. F. Pedersen, and J. T. Cullen. 2014. Undocumented water column sink for cadmium in open ocean oxygen-deficient zones. *Proc. Natl. Acad. Sci. USA* **111**: 6888–6893. doi:[10.1073/pnas.1402388111](https://doi.org/10.1073/pnas.1402388111)
- Janssen, D. J., W. Abouchami, S. J. G. Galer, and J. T. Cullen. 2017. Fine-scale spatial and interannual cadmium isotope variability in the subarctic northeast Pacific. *Earth Planet. Sci. Lett.* **472**: 241–252.
- John, S. G., J. Helgoe, and E. Townsend. 2018. Biogeochemical cycling of Zn and Cd and their stable isotopes in the Eastern Tropical South Pacific. *Mar. Chem.* **201**: 256–262. doi:[10.1016/j.marchem.2017.06.001](https://doi.org/10.1016/j.marchem.2017.06.001)
- Knowles, R. 1982. Denitrification. *Microbiol. Rev.* **46**: 43–70.
- Lagerström, M. E., M. P. Field, M. Séguret, L. Fischer, S. Hann, and R. M. Sherrell. 2013. Automated on-line flow-injection ICP-MS determination of trace metals (Mn, Fe, Co, Ni, Cu and Zn) in open ocean seawater: Application to the GEOTRACES program. *Mar. Chem.* **155**: 71–80. doi:[10.1016/j.marchem.2013.06.001](https://doi.org/10.1016/j.marchem.2013.06.001)
- Lam, P. J., and J. K. B. Bishop. 2008. The continental margin is a key source of iron to the HNLC North Pacific Ocean. *Geophys. Res. Lett.* **35**: 1–5. doi:[10.1029/2008GL033294](https://doi.org/10.1029/2008GL033294)
- Lam, P. J., M. I. Heller, P. E. Lerner, J. W. Moffett, and K. N. Buck. 2020. Unexpected source and transport of iron from the deep Peru margin. *ACS Earth Space Chem.* **4**: 977–992. doi:[10.1021/acsearthspacechem.0c00066](https://doi.org/10.1021/acsearthspacechem.0c00066)
- Landing, W. M., and K. W. Bruland. 1980. Manganese in the North Pacific. *Earth Planet. Sci. Lett.* **49**: 45–56. doi:[10.1016/0012-821X\(80\)90149-1](https://doi.org/10.1016/0012-821X(80)90149-1)
- Liu, X., and F. J. Millero. 2002. The solubility of iron in seawater. *Mar. Chem.* **77**: 43–54. doi:[10.1016/S0304-4203\(01\)00074-3](https://doi.org/10.1016/S0304-4203(01)00074-3)
- Luther, G. W., III, J. Wu, and J. B. Cullen. 1995. Redox chemistry of iodine in seawater: frontier molecular orbital theory considerations. ACS Publications.
- Löscher, B. M., J. T. M. De Jong, and H. J. W. De Baar. 1998. The distribution and preferential biological uptake of cadmium at 6°W in the Southern Ocean. *Mar. Chem.* **62**: 259–286. doi:[10.1016/S0304-4203\(98\)00045-0](https://doi.org/10.1016/S0304-4203(98)00045-0)
- McLennan, S. M. 1989. Rare earth elements in sedimentary rocks: Influence of provenance and sedimentary processes, p. 169–200. *In* *Geochemistry and mineralogy of rare earth elements*. De Gruyter.
- Measures, C. I., W. M. Landing, M. T. Brown, and C. S. Buck. 2008. A commercially available rosette system for trace metal—Clean sampling. *Limnol. Oceanogr. Methods* **6**: 384–394.
- Moffett, J. W. 1990. Microbially mediated cerium oxidation in sea water. *Nature* **345**: 421–423. doi:[10.1038/345421a0](https://doi.org/10.1038/345421a0)
- Moffett, J. W. 1994. A radiotracer study of cerium and manganese uptake onto suspended particles in Chesapeake Bay. *Geochim. Cosmochim. Acta* **58**: 695–703. doi:[10.1016/0016-7037\(94\)90499-5](https://doi.org/10.1016/0016-7037(94)90499-5)
- Moffett, J. W., and C. R. German. 2020. Distribution of iron in the Western Indian Ocean and the Eastern tropical South Pacific: An inter-basin comparison. *Chem. Geol.* **532**: 119334. doi:[10.1016/j.chemgeo.2019.119334](https://doi.org/10.1016/j.chemgeo.2019.119334)
- Moffett, J. W., and J. Ho. 1996. Oxidation of cobalt and manganese in seawater via a common microbially catalyzed pathway. *Geochim. Cosmochim. Acta* **60**: 3415–3424. doi:[10.1016/0016-7037\(96\)00176-7](https://doi.org/10.1016/0016-7037(96)00176-7)
- Morel, F. M. M., A. J. Milligan, and M. A. Saito. 2003. Marine bioinorganic chemistry: The role of trace metals in the oceanic cycles of major nutrients. *Treat. Geochem.* **6**: 625.
- Moriyasu, R., N. Evans, K. M. Bolster, D. S. Hardisty, and J. W. Moffett. 2020. The distribution and redox speciation of iodine in the eastern tropical North Pacific Ocean. *Global Biogeochem. Cycl.* **34**: 1–23. doi:[10.1029/2019GB006302](https://doi.org/10.1029/2019GB006302)
- Morton, P. L., and others. 2019. Shelf inputs and lateral transport of Mn, Co, and Ce in the western north Pacific Ocean. *Front. Mar. Sci.* **6**: 591. doi:[10.3389/fmars.2019.00591](https://doi.org/10.3389/fmars.2019.00591)
- Noble, A. E., and others. 2012. Basin-scale inputs of cobalt, iron, and manganese from the Benguela-Angola front to the South Atlantic Ocean. *Limnol. Oceanogr.* **57**: 989–1010. doi:[10.4319/lo.2012.57.4.0989](https://doi.org/10.4319/lo.2012.57.4.0989)

- Ohnemus, D. C., R. Torrie, and B. S. Twining. 2019. Exposing the distributions and elemental associations of scavenged particulate phases in the ocean using basin-scale multi-element data sets. *Global Biogeochem. Cycl.* **33**: 725–748. doi:10.1029/2018GB006145
- Peters, B. D., W. J. Jenkins, J. H. Swift, C. R. German, J. W. Moffett, G. A. Cutter, M. A. Brzezinski, and K. L. Casciotti. 2018. Water mass analysis of the 2013 US GEOTRACES eastern Pacific zonal transect (GP16). *Mar. Chem.* **201**: 6–19. doi:10.1016/j.marchem.2017.09.007
- Pierotti, D., and R. A. Rasmussen. 1980. Nitrous oxide measurements in the eastern tropical Pacific Ocean. *Tellus* **32**: 56–72.
- Resing, J. A., P. N. Sedwick, C. R. German, W. J. Jenkins, J. W. Moffett, B. M. Sohst, and A. Tagliabue. 2015. Basin-scale transport of hydrothermal dissolved metals across the South Pacific Ocean. *Nature* **523**: 200–203. doi:10.1038/nature14577
- Roshan, S., and T. DeVries. 2021. Global contrasts between oceanic cycling of cadmium and phosphate. *Global Biogeochem. Cycl.* **35**: e2021GB006952. doi:10.1029/2021gb006952
- Saager, P. M., H. J. W. De Baar, and P. H. Burkil. 1989. Manganese and iron in Indian Ocean waters. *Geochim. Cosmochim. Acta* **53**: 2259–2267.
- Schlitzer, R., and others. 2018. The GEOTRACES intermediate data product 2017. *Chem. Geol.* **493**: 210–223. doi:10.1016/j.chemgeo.2018.05.040
- Slater, F. R., E. Boyle, and J. M. Edmond. 1976. On the marine geochemistry of nickel. *Earth Planet. Sci. Lett.* **31**: 119–128.
- Shiller, A. M. 1997. Manganese in surface waters of the Atlantic Ocean. *Geophys. Res. Lett.* **24**: 1495–1498. doi:10.1029/97GL01456
- Siebe, C., J. C. Komorowski, C. Navarro, J. McHone, H. Delgado, and A. Cortés. 1995. Submarine eruption near Socorro Island, Mexico: Geochemistry and scanning electron microscopy studies of floating scoria and reticulite. *J. Volcanol. Geotherm. Res.* **68**: 239–271. doi:10.1016/0377-0273(95)00029-1
- Sieber, M., T. M. Conway, G. F. de Souza, H. Obata, S. Takano, Y. Sohrin, and D. Vance. 2019. Physical and biogeochemical controls on the distribution of dissolved cadmium and its isotopes in the Southwest Pacific Ocean. *Chem. Geol.* **511**: 494–509.
- Sunda, W. G., S. A. Huntsman, and G. R. Harvey. 1983. Photo-reduction of manganese oxides in seawater and its geochemical and biological implications. *Nature* **301**: 234–236. doi:10.1038/301234a0
- Sundby, B., L. G. Anderson, P. O. J. Hall, Å. Iverfeldt, M. M. R. van der Loeff, and S. F. G. Westerlund. 1986. The effect of oxygen on release and uptake of cobalt, manganese, iron and phosphate at the sediment-water interface. *Geochim. Cosmochim. Acta* **50**: 1281–1288. doi:10.1016/0016-7037(86)90411-4
- Tiano, L., E. Garcia-Robledo, T. Dalsgaard, A. H. Devol, B. B. Ward, O. Ulloa, D. E. Canfield, and N. Peter Revsbech. 2014. Oxygen distribution and aerobic respiration in the north and south eastern tropical Pacific oxygen minimum zones. *Deep. Res. Part I Oceanogr. Res. Pap.* **94**: 173–183. doi:10.1016/j.dsr.2014.10.001
- Vedamati, J., C. Chan, and J. W. Moffett. 2015. Distribution of dissolved manganese in the Peruvian upwelling and oxygen minimum zone. *Geochim. Cosmochim. Acta* **156**: 222–240. doi:10.1016/j.gca.2014.10.026
- Wu, J., and S. Roshan. 2015. Cadmium in the North Atlantic: Implication for global cadmium-phosphorus relationship. *Deep. Res. Part II Top. Stud. Oceanogr.* **116**: 226–239. doi:10.1016/j.dsr2.2014.11.007
- Wuttig, K., and others. 2019. Critical evaluation of a seaFAST system for the analysis of trace metals in marine samples. *Talanta* **197**: 653–668. doi:10.1016/j.talanta.2019.01.047
- Yang, S.-C., and others. 2021. Lack of redox cycling for nickel in the water column of the eastern tropical North Pacific oxygen deficient zone: Insight from dissolved and particulate nickel isotopes. *Geochim. Cosmochim. Acta.* **309**: 235–250.
- Yang, S.-C., J. Zhang, Y. Sohrin, and T.-Y. Ho. 2018. Cadmium cycling in the water column of the Kuroshio-Oyashio extension region: Insights from dissolved and particulate isotopic composition. *Geochim. Cosmochim. Acta* **233**: 66–80. doi:10.1016/j.gca.2018.05.001
- Zhang, Y., L. Li, J. Ren, H. He, R. Zhang, L. Zhao, J. Zhang, and M. Zhao. 2021. Distribution and influencing factors of dissolved manganese in the Yellow Sea and the East China Sea. *Mar. Chem.* **234**: 104002. doi:10.1016/j.marchem.2021.104002
- Zheng, X.-Y., Y. Plancherel, M. A. Saito, P. M. Scott, and G. M. Henderson. 2016. Rare earth elements (REEs) in the tropical South Atlantic and quantitative deconvolution of their non-conservative behavior. *Geochim. Cosmochim. Acta* **177**: 217–237.

Acknowledgments

The authors thank the captain and crew of the R/V Revelle RR1804-1805 and the chief scientists Richard Keil and Allan Devol for their help during the cruise. This manuscript greatly benefitted from feedback from the Associate Editor Prof. Vanessa Hatje and two anonymous reviewers. This research was supported by the US National Science Foundation Grants OCE-1736896 to S.G.J. and OCE-1636332 to S.G.J. and J.W.M.

Conflict of Interest

None declared.

Submitted 25 May 2022

Revised 18 October 2022

Accepted 04 December 2022

Associate editor: Vanessa Hatje